Supporting information

Fabrication of an Advanced Asymmetric Supercapacitor based on Three-Dimensional Copper-Nickel-Cerium-Cobalt Quaternary Oxide and GNP for Energy Storage Application

Lopamudra Halder, Anirban Maitra, Amit Kumar Das, Ranadip Bera, Sumanta Kumar Karan, Sarbaranjan Paria, Aswini Bera, Suman Kumar Si, and Bhanu Bhusan Khatua*

Materials Science Centre, Indian Institute of Technology Kharagpur, Kharagpur- 721302, West Bengal, India.

***Corresponding Author**

Dr. B. B. Khatua (Email:khatuabb@matsc.iitkgp.ernet.in).

Materials Science Centre, Indian Institute of Technology, Kharagpur –721302, India.

Tel.:+91-3222-283982

S1. TEM-EDS mapping analysis

The TEM-elemental mapping analysis was performed to demonstrate the distribution of all the elements in the nanosheet. The as-appeared signals in the EDX spectrum indicate the weight and atomic percent of all four elements Cu, Co, Ni, Ce within the quaternary oxide.

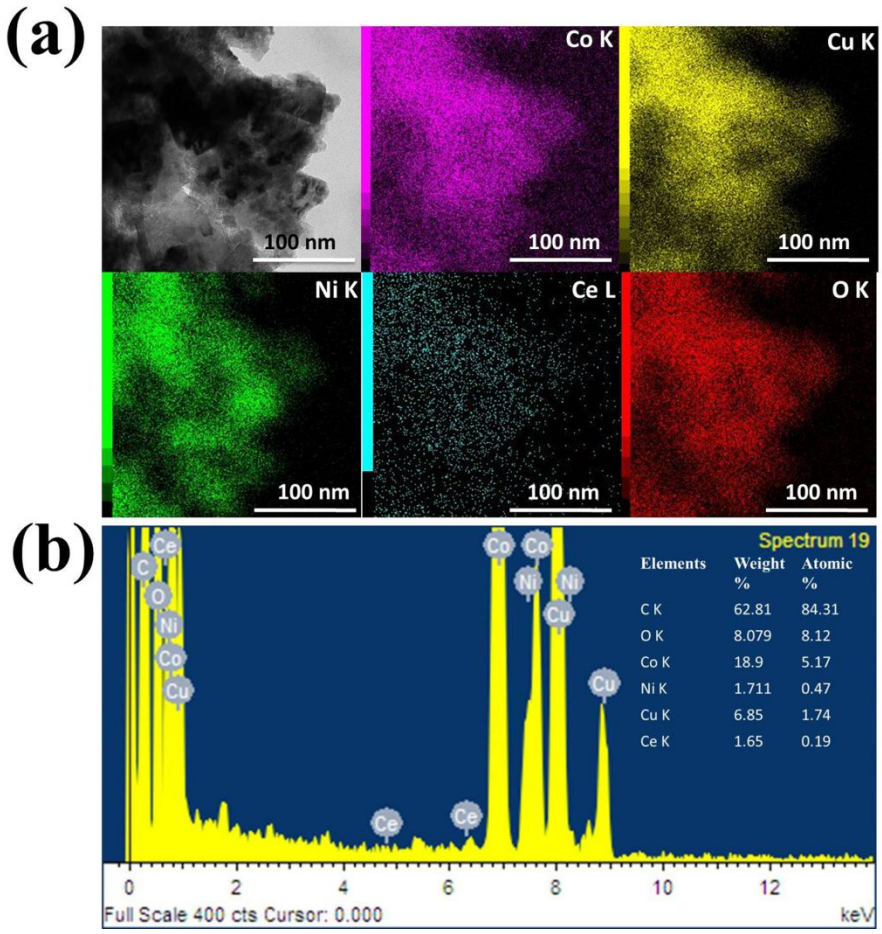

Figure S1. (a) TEM-EDX mapping images, (b) TEM-EDS spectrum of Cu-Ni-Ce-Co oxide

S2. Surface area and pore size distribution analysis.

The specific surface area was determined through the BET analysis and Pore- size distribution of the electrode materialhas been carried out by BJH model based on adsorption desorption

curve.Figure S2a represents N_2-adsorption desorption isotherm of Cu-Ni-Ce-Co oxide. The isotherm reveals characteristic of type-IV pattern (under IUPAC convention), with a distinct hysteresis loop within the region 0.8−1.0 P/P_0 which mainly signifies the presence of ample mesopores in the nanosheet. The BET specific surface area was found to be 86.9 $m^2\ g^{-1}$. Figure S2b exhibits a narrow pore-size distribution of the hybrid electrode material which is mainly concentrated in the range of 1− 6 nm. The average pore diameter was calculated to be 4.34 nm which satisfy the criteria of mesoporous material accurately. The pore size is optimal for easy diffusion of electrolytic ions through the nanosheets and therefore results in a fast charge-transfer process. This eventually improves the specific capacitance value. The high surface area along with mesoporous feature permits complete exposure of electroactive sites to KOH electrolyte, which eventually increases electrode-electrolyte interaction. Moreover, shortening of electron and ion diffusion path initiates fast charge transfer process.

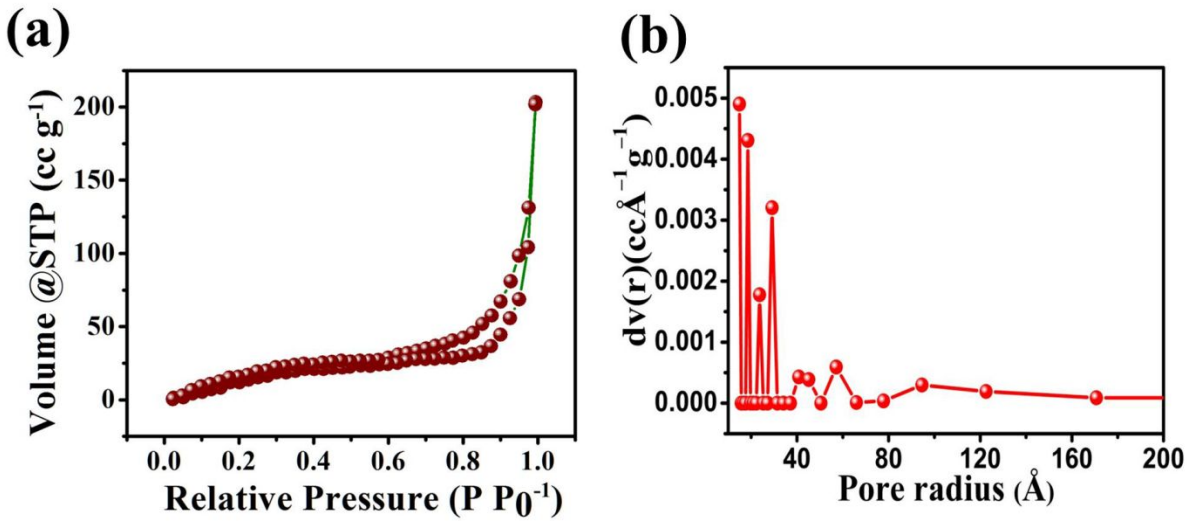

Figure S2. (a) Nitrogen adsorption-desorption isotherm and (b) BJH pore size distribution plot of Cu-Ni-Ce-Co oxide.

S3. Electrochemical performance of GNP as negative electrode.

Graphene nano-platelet (GNP) coated stainless steel (GNP@SS) has been chosen here as negative electrode. CV and GCD analysis were performed in three-electrode cell configuration using 1 M KOH electrolyte solution with platinum and saturated calomel electrode (SCE) as counter and reference electrodes respectively. Figure S3a represents cyclic voltammetry (CV) plots of GNP at a various scan rates in a voltage window of −1 to 0 V. The CV plot demonstrates EDLC type charge-storage behavior. Figure S3b depicts GCD plot of GNP at different current densities within the potential window of −1 to 0. The perfect triangular shape of the GCD plots validates the EDLC contribution of GNP as negative electrode material. The C_s values were calculated according to the eq 1, were found to be 163, 160.3, 156.7, 151.06, 149.5 F g^{-1} at 1, 2, 4, 8, 10 A g^{-1} current densities respectively, signifying a good rate capability of GNP.

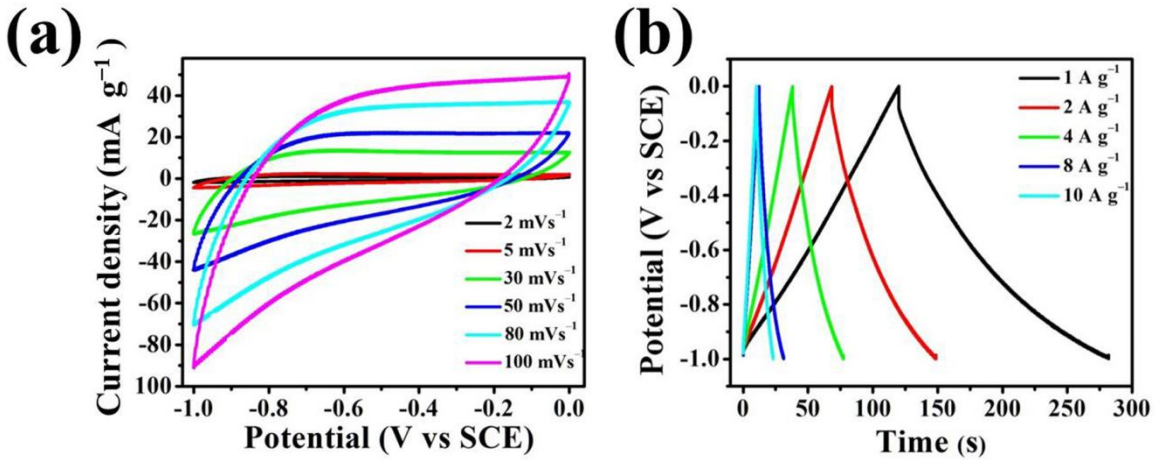

Figure S3.(a) CV and (b) GCD plots of GNP.

S4. Electrochemical performances of prepared electrode materials.

The capacitive performance for various mixed oxides combination i.e. Cu-Ni oxide, Ni-Co oxide, Cu-Ce oxide, Ce-Co oxide, Cu-Ce-Co oxide, Ce-Ni-Co oxide, and Cu-Ni-Ce oxide has been evaluated in three- electrode cell configuration. The CV and GCD analysis were carried out

in 1 M KOH electrolyte solution. The CV plots of all the electrode materials at a fixed 5 mV s^{-1} scan rate has been represented in Figure S4a. The ultimate supercapacitive performance was evaluated from GCD analysis (as in Figure S4b). The C_s values were calculated from the discharge plots of the electrode materials accordingly from the following eq:

$$C_s = \frac{i \times \Delta t}{m \times \Delta V}$$

The C_s values of 2050 F g^{-1} (for Ce-Ni-Co oxide), 1878 F g^{-1} (for Cu-Ni-Ce oxide), 1603 F g^{-1} (for Cu-Ce-Co oxide), 920 F g^{-1} (for Ni-Co oxide), 770 F g^{-1} (for Cu-Ni oxide), 442.5 F g^{-1} (for Ce-Co oxide), 163.2 F g^{-1} (for Cu-Ce oxide) were achieved at 1 A g^{-1} current density. Figure S4c reveals the comparative electrochemical performances of all the electrode materials with previously reported electrode materials in this work.

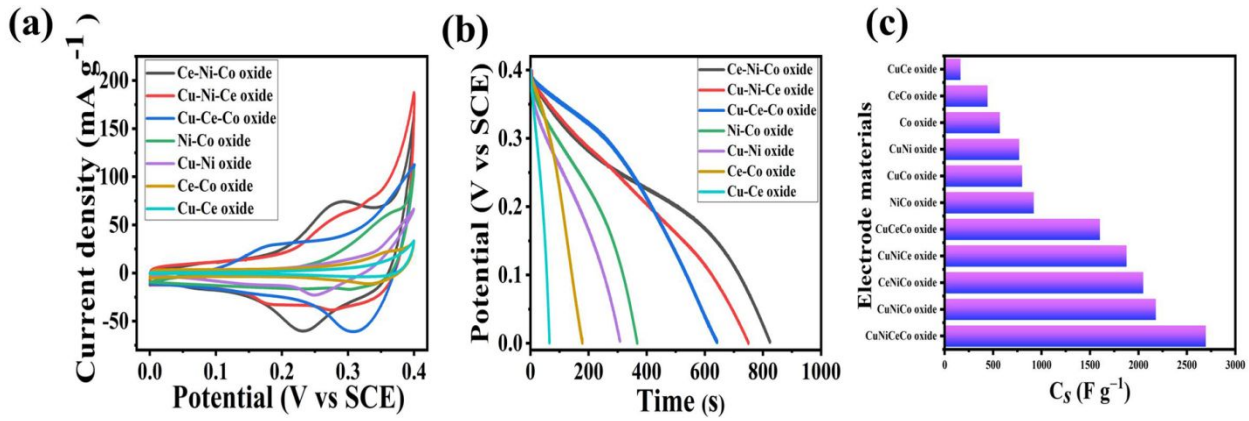

Figure S4 Comparison of (a) CV profiles at 5 mV s^{-1} scan rate, (b) GCD plots at 1 A g^{-1} of different mixed metal oxides, (c) variation of specific capacitance of as synthesized electrode materials at 1 A g^{-1}.

S5. Comparison of ASC device performance employing other different mixed oxides as positive electrodes.

The four ASC devices have been fabricated using Cu-Ni-Ce-Co oxide, Cu-Ni-Co oxide, Cu-Co oxide, and Co oxide as positive electrode materials respectively. In all cases, GNP is the negative electrode material. CV and GCD analysis in two- electrode configuration were carried out in 1 M aqueous KOH electrolyte using Whatman 40 filter paper as separator. Figure S5a and b represents the comparative CV profiles at 2 mV s^{-1} scan rate and GCD plots 1 A g^{-1} current density of all the different ASCs. The mass ratios were found to be 0.1818, 0.188, 0.512, 0.73 for ASCs assembled with Cu-Ni-Ce-Co oxide, Cu-Ni-Co oxide and Cu-Co oxide and Co oxide as positive electrode materials respectively and GNP as negative electrode. The C_s values were achieved using equation $C_s = \frac{i \times \Delta t}{m \times \Delta V}$

The C_s values of 183.3, 152, 89.2, 43 F g^{-1} were calculated from discharge plots of Cu-Ni-Ce-Co oxide//GNP, Cu-Ni-Co oxide//GNP and Cu-Co oxide//GNP and Co oxide//GNP ASC devices respectively at 1 A g^{-1} current density. Figure S5c depicts comparison of C_s values at 1 A g^{-1} achieved from different ASCs.

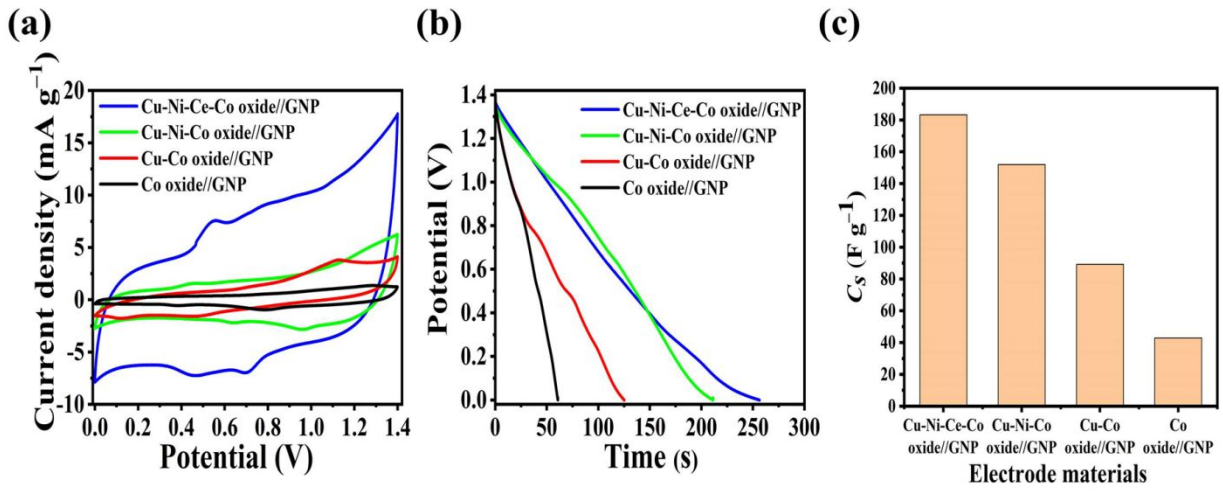

Figure S5 Comparative (a) CV profiles at 2 mV s^{-1} scan rate, (b) GCD plots at 1 A g^{-1} current density of ASCs employing different mixed metal oxides as positive electrodes and GNP as negative electrode material, (c) comparison of specific capacitance obtained from different ASCs.